

# A Discrete-time Self-clocking Complex Electromechanical $\Sigma\Delta$ Gyroscope with Quadrature Error Cancellation

Fang Chen, Dacheng Xu, Wei Zhou, Michael Kraft, and Xinxin Li

**Abstract**— In this work, an new self-clocking electro-mechanical sigma-delta modulated ( $\Sigma\Delta$ ) quadrature error cancellation scheme for MEMS resonant gyroscopes was presented. The proposed techniques allow gyroscope sense mode in-phase and quadrature-phase sigma-delta decomposition to efficiently realize high-order sigma-delta noise shaping and error suppression. The system was also design with a self-clocking calibration scheme to provided temperature-independent turn-on bias output. Simulation results proved its robustness and nonlinearity optimized, which achieved over 80dB attenuation of quadrature error. The hardware implementation based on a integrated circuit system and a wheel gyroscope has been demonstrated. Measurement results indicate an inherent loop quadrature cancellation scheme and show a sub-1°/hr bias instability (BI), with 5.5X and 3X improvement of BI and angle random walk (ARW) compared with a conventional single-loop  $\Sigma\Delta$  gyroscope system. Combined with real-time self-clocking control, it yields an improvement of turn on bias error (1800s) and output linearity, reaching 1°/h and 0.021%, respectively.

**Index Terms**—MEMS Gyroscopes, Complex Sigma-delta modulated, Noise shaping, Quadrature error, Cancellation

## I. INTRODUCTION

MICROMACHINED vibratory gyroscope output bias stability or drift, has still hindered their penetration into high-end tactical or navigation markets, where high bias stability and scale factor stability are required over long periods of time to avoid positioning and heading errors [1]. Improving the stability of MEMS gyroscope has created new challenges in the their design and fabrication, as well as the interface and control circuits. Electrostatic force-rebalancing can be used to reduce the influence of the mechanical parameters of the gyroscope

and frequency matching errors. However, there are still other unwanted effects, such as the stiffness and damping coupling factor and the variation of the characteristics with temperature and vibration [2]. Most of the amplitude modulated (AM) gyroscope performance parameters are still susceptible to environmental changes; therefore, stability is still not sufficient for some high performance applications. Electromechanical sigma-delta modulated force-rebalancing in the sense mode can preserve advantages of closed-loop operation and concurrently produce a digital output based on a pulse density or width modulated (PDM or PWM) bitstream [3-5]. This transforms the sensing information in the feedback amplitude into information in time and thus making it suitable for integration. Since the feedback voltage of electromechanical sigma-delta modulator can only have discrete levels and nonlinearity of the quantizer as the input amplitude increase, this operation is inherently exist non-linear. Furthermore, electromechanical sigma-delta modulated force-rebalancing still represents a very effective technique to implement high precision MEMS gyroscope [6].

Since current micromachining technologies do not allow gyroscope sensing elements with perfectly isotropic working modes, non-ideal effects are still inevitable. Even if the mass of the gyroscope can be trimmed by laser machining [7], this is a time-consuming and expensive approach. The bias output of a conventional sigma-delta gyroscope includes two main error sources: quadrature and in-phase errors. Quadrature errors have a relative phase of 90° with respect to the Coriolis force, and they can be rejected in a phase-sensitive demodulation process. However, in practice quadrature errors still leak into the sense channel; therefore, the rate output will be contaminated and thus drastically degrade the output bias drift. The in-phase errors are typically much smaller than the quadrature errors, but are in-phase with the Coriolis force. The dominant contributors of in-phase errors are electrical signal feedthrough and anisotropic damping. It is problematic to distinguish in-phase errors from the rate gyroscope in conventional approaches as it requires more sophisticated continuous monitoring techniques.

Complete suppression of the quadrature motion requires a force applied to the sense mode, which exactly is in-phase with the drive displacement. In some literatures, the quadrature error cancellation approach is normally done by careful design; examples include using specially designed mechanical levers [8] and using some dedicated mechanical electrodes on the sensor to eliminate quadrature error motion [9]. However, it is not

This work was supported in part by the National Natural Science Foundation of China under Grant 61974156, 61504159 and 61674160; in part by the Natural Science Foundation of Shanghai under Grant 19ZR1467300.

F. Chen, W. Zhou, and X. Li are with the State Key Laboratory of Transducer Technology, Shanghai Institute of Microsystem and Information Technology, Chinese Academy of Sciences, Shanghai, China (e-mail: fangchen@mail.sim.ac.cn, xxli@mail.sim.ac.cn).

D. Xu and X. Li is with the School of Electronic and Information Engineering, Soochow University, Suzhou 215006, China.

M. Kraft is with MICAS Group, Catholic University of Leuven, 3000 Leuven, Belgium.

applicable to generic gyroscope sensing elements since the mechanical design requires additional dedicated electrodes. Electrical error cancellation on the other hand benefits from the flexibility and low cost of electrical signal processing to provide in-run cancellation of gyroscope quadrature error, that can be integrated in a compact sensor system.

This paper expands on preliminary research presented in [10] by taking advantage of a complex (or quadrature) sigma-delta modulator ( $\Sigma\Delta$ ) closed-loop sensing scheme. It facilitates in-run self-clocking, providing an inherent cancellation of the gyroscope quadrature error as well as suppression of turn-on bias drift and in-phase errors. A digital gyroscope system that overcomes the performance limits of conventional sigma-delta gyroscope architecture is described in the following. Both the conventional single-loop and the proposed self-clocking  $\Sigma\Delta$  with optimized architecture are presented. In this operation mode, the quadrature error of MEMS gyroscope was seriously depressed. Furthermore, an in-run self-clocking mode enabled minimum gyroscope turn-on bias drift variation in the presence of environmental parameter changes, such as temperature. The working principle of the proposed complex electromechanical  $\Sigma\Delta$  gyroscope system is presented in section II, followed by an analysis of its modeling, robustness and non-idealities. Section III describes detailed simulations of the gyroscope system. Implementation and experimental results are presented in Section IV, verifying the advantages of the proposed approaches. Finally, discussions and conclusions are given in Section V.

## II. SYSTEM DESIGN AND ANALYSES

### A. Review of Conventional $\Sigma\Delta$ gyroscopes

Fig.1 shows the generic architecture of a single loop force rebalancing electromechanical  $\Sigma\Delta$  gyroscope system, derived from the architecture of conventional electronic sigma-delta modulators. This is a hybrid nonlinear system comprising components in both the mechanical as well as the electrical domain. The  $C/V$  block senses the capacitance variation due to the input signal and transforms it to a voltage signal then can be processed by the subsequent electronic filters. The output of the quantizer, which represents the  $\Sigma\Delta$  output, is applied to the sensor actuation electrodes creating an electrostatic feedback force. The  $V/F$  block represents the electrostatic force resulting from the feedback bitstream which contains both the in-phase Coriolis force and quadrature-phase error information. It can be noted that, in some systems, only the gyroscope element serves as the  $\Sigma\Delta$  loop filter, which results in increased quantization noise leading to decreased resolution. Therefore, higher-order, electromechanical  $\Sigma\Delta$  based on local feed-forward (FF) or distributed feedback (DF) sigma-delta architectures are the most practical architectures for micromachined gyroscopes [3].

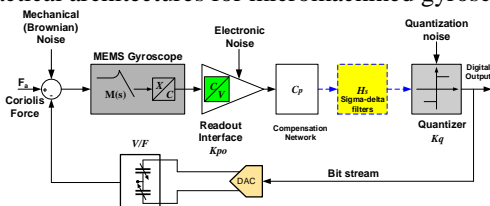


Fig. 1. Typical high-order EM- $\Sigma\Delta$  interface system for a MEMS gyroscope [3].

The digital output signal from the EM- $\Sigma\Delta$  interface is a bit stream generated by a binary quantizer. The generated feedback voltage signal applied to the differential actuation electrodes is either corresponding to logic '0' or logic '1', depending on the reference voltage  $V_{REF}$  of the  $\Sigma\Delta$  system. Hence, the actuation signal assumes one of two possible states (binary actuation). The gyroscope full-scale feedback force and the corresponding full-scale input acceleration is given by

$$F_{full-scale} = \frac{1}{2} \frac{C_{fb}}{x_0} V_{REF}^2 \quad (1)$$

$$a_{full-scale} = \frac{1}{2} \frac{1}{m} \frac{C_{fb}}{x_0} V_{REF}^2 \quad (2)$$

where  $C_{fb}$  is the feedback actuation capacitance,  $m$  is the effective gyroscope proof mass, and  $x_0$  is the feedback capacitance gap. Although only linear two points of the quadratic  $V/F$  relation are exercised, it still can suffer from nonlinear harmonics in the output spectrum and thus limiting the total signal-to-noise ratio. An expression of the gyroscope system output bit stream can be derived as:

$$Y_{bit} = STF(F_{in}) + QNTF(Q_{in}) + ENTf(E_{in}) \quad (3)$$

where  $STF$  is the input signal transfer function;  $QNTF$  is the multi-bit or single-bit quantization noise transfer function, respectively; and  $ENTf$  is the electronic noise transfer function.  $F_{in}$  includes the input Coriolis and quadrature error force,  $Q_{in}$  and  $E_{in}$  are the quantization and electronic noise, respectively.

The simulated bitstream output power spectral density (PSD) of a single-loop EM- $\Sigma\Delta$  gyroscope is shown in Fig.2. There is a quadrature error signal at the drive center frequency, while the Coriolis signal appears as two side-band peaks. Assuming  $x(t)$  is the drive displacement, quadrature error displacement  $y_{Quad}$  and quadrature force  $F_q$  can be expressed as

$$x(t) = x_0 \sin(\omega_x t) \quad (4)$$

$$y_{Quad}(t) = -\varepsilon x(t) \quad (5)$$

$$F_q(t) = \varepsilon x_0 \omega_x^2 \sin(\omega_x t) \quad (6)$$

where  $\varepsilon$  is the coupling coefficient between drive and sense displacements. Since the Coriolis signal is small, the quadrature error signal can dominate the output. Reduction of the full scale signal and hence the high dynamic range is achieved by cancelling the quadrature error. If the  $\Sigma\Delta$  gyroscope system quadrature error signal cannot be cancelled, the force feedback loop needs to accommodate it in its full-scale range in order to rebalance the proof mass.

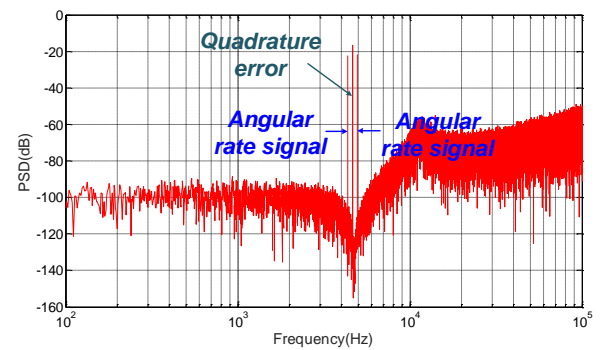


Fig. 2. Power spectral density (PSD) of the output bitstream of a high-order single loop SDM gyroscope.

## B. Design of EM- $\Sigma\Delta$ with quadrature cancellation

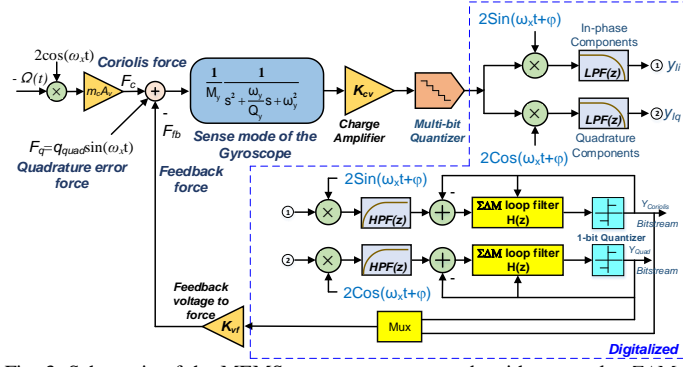


Fig. 3. Schematic of the MEMS gyroscope sense mode with a complex  $\Sigma\Delta$  control loop. Coriolis force and Quadrature error are orthogonally demodulated, and re-modulated in two EM- $\Sigma\Delta$  loops.

The block diagram of the proposed gyroscope system with a complex EM- $\Sigma\Delta$  is shown in Fig.3. There are two control loops termed in-phase and quadrature-phase loop, employed to force balance the Coriolis force and quadrature error, respectively. The sense mode displacement is translated into a capacitance change, which is detected using a pick-off circuit with a conversion gain  $K_{cv}$  (ratio of change in capacitance to voltage). The sensing signal is firstly digitized by a multi-bit quantizer and then passed to an phase-sensitive demodulation block. The resulting rectified signal is passed through a low-pass filter to obtain the amplitude information of the quadrature component  $Y_{iq}(t)$  and the in-phase component  $Y_{ii}(t)$ .  $\Omega(t)$  and  $q_{quad}$  are input angular rate and equivalent quadrature error coupling amplitude, respectively.  $F_c(t)$ ,  $F_q(t)$  and  $F_{fb}(t)$  represent Coriolis force, quadrature force and counter rebalanced force, respectively.  $m_c$  represents the effective proof mass and  $A_v$  the amplitude of the drive velocity.  $\omega_y$  and  $Q_y$  are the sense mode resonant frequency and quality factor, respectively.

Assume that the velocity of the drive mode is

$$v(t) = A_v \cos(\omega_x t) \quad (7)$$

the Coriolis force and quadrature force can be expressed as

$$F_c(t) = 2m_c A_v \Omega \cos(\omega_x t) \quad (8)$$

$$F_q(t) = q_{quad} \sin(\omega_x t) \quad (9)$$

Thus, the pick-off output voltage can be obtained as

$$y(t) = \frac{2m_c A_v \Omega}{m_y} [A_1 \cos(\omega_x t) + B_1 \sin(\omega_x t)] \quad (10)$$

$$+ \frac{q_{quad}}{m_y} [A_1 \sin(\omega_x t) + B_1 \cos(\omega_x t)]$$

where  $m_c$  is the sense mass. The variables  $A_1$  and  $B_1$  are defined in eqs. (?)-(?).

$$A_1 = \frac{\omega_y^2 - \omega_x^2}{(\omega_y^2 - \omega_x^2)^2 + \omega_y^2 \omega_x^2 / Q_y^2} \quad (11)$$

$$B_1 = \frac{-\omega_y \omega_x / Q_y}{(\omega_y^2 - \omega_x^2)^2 + \omega_y^2 \omega_x^2 / Q_y^2} \quad (12)$$

The pick-off output voltage  $y(t)$  is quantized and demodulated by a signal of  $2\sin(\omega_x t + \phi)$  and  $2\cos(\omega_x t + \phi)$ , respectively. Then, they are both passed through a low-pass filter  $LPF(z)$  to remove the high frequency components, as shown in Fig.3. Hence, the

in-phase  $Y_{ii}(t)$  and quadrature signals  $Y_{iq}(t)$  are described as

$$y_{ii}(t) = \Omega \frac{2m_c A_v k_{cv}}{m_y} (A_1 \sin(\phi) - B_1 \cos(\phi)) \quad (13)$$

$$y_{iq}(t) = \frac{q_{quad}}{m_y} (B_1 \cos(\phi) - A_1 \sin(\phi)) \quad (14)$$

Since the Coriolis force signal due to the input angular rate and quadrature error forces are modulated to the vicinity of the drive mode resonant frequency, a re-modulation process is necessary to construct the in-phase loop and quadrature cancellation loops, respectively. After that, two identical band-pass  $\Sigma\Delta$  architectures are embedded within the in-phase and quadrature-phase loops for re-modulation, which also takes advantage of a dual quantization mechanism. Both band-pass EM- $\Sigma\Delta$ s are designed in such a way that its center frequency coincides with the drive mode resonant frequency, since the sense mode output signal (due to the Coriolis force) and the quadrature error force are modulated at the drive frequency. Therefore, in-phase  $Y_{ii}(t)$  and quadrature-phase  $Y_{iq}(t)$  signals are moved to the center frequency of the band-pass EM- $\Sigma\Delta$ s. Fig.4 shows a frequency response of a low-pass and a band-pass sigma-delta modulator.  $f_r$  and  $f_{bw}$  are the resonant frequency and signal bandwidth of the gyroscope, respectively. To achieve the same signal-to-noise ratio (SNR) for a given order, it is obvious that the sampling frequency of the low-pass modulator,  $f_{s1}$  must be chosen considerably higher than for a band-pass modulator,  $f_{s2}$ .

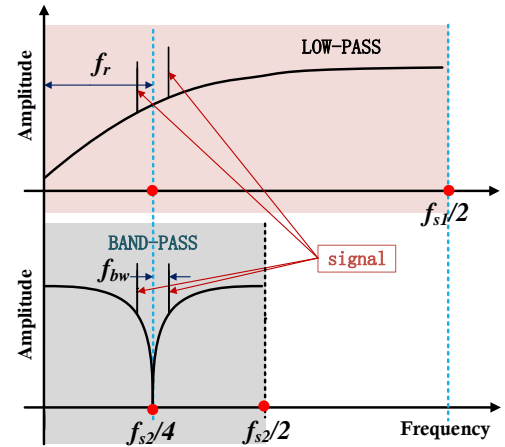


Fig. 4. Comparison of the frequency response for a low-pass and band-pass sigma-delta modulator.

Fig.5 shows a block diagram of the equivalent in-phase and quadrature 4<sup>th</sup>-order  $\Sigma\Delta$  loops, incorporating the gyroscope mechanical resonator. There is a lead phase compensator  $C_p(z) = A(1 - \alpha z^{-1})$  located before the electronic modulator, which include two cascading integrators  $H_i(z)$  ( $i=1,2$ ) with a transfer function of  $H_1(z) = (z/z-1)$  and  $H_2(z) = (1/z-1)$ . The gain constants  $A_i$ ,  $B_i$ ,  $C_i$ ,  $D_i$ , ( $i=1, 2$ ) are used for scaling the modulator output amplitude if the mechanical parameters of the gyroscope vary due to unavoidable micro-fabrication tolerances. The local feedback paths produce a notch for faster decay in the stop-band and thus further suppress the multi-bit quantization noise presented here.  $Y_{Cor}(n)$  and  $Y_{Quad}(n)$  are outputs of the in-phase and quadrature-phase channel bitstreams, respectively. The adopted sigma-delta architecture is derived by applying an

advanced design methodology based on optimization and stability criteria which is described in more detail in [11-13]. All values of the gain constants are given in the Table I.

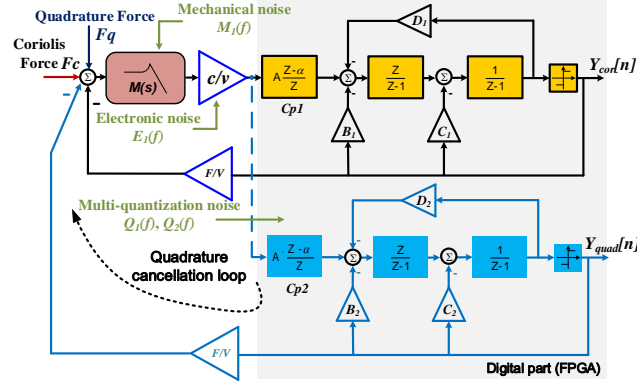


Fig. 5. Simulink model of the Coriolis detection and quadrature cancellation loops.

TABLE I  
MAIN GAIN PARAMETERS OF THE SIMULATION SYSTEM

Parameter	In-phase	Quadrature-phase
Moment of inertia ( $\mu\text{g} \times \mu\text{m}^2$ )	$8.86 \times 10^6$	$8.86 \times 10^6$
Quality factor ( $Q_y$ )	10000	10000
Resonance frequency $f_y$ (Hz)	4700	4700
Pick-off gain $K_{cv}$ (V/F)	$1.58 \times 10^{13}$	$1.58 \times 10^{13}$
Compensator gain $A$	40~100	40~100
Local feedback gain $B$	0.2467	0.2467
Local feedback gain $C$	0.5566	0.5566
Feed forward gain $D$	0.0022	0.0022
Sampling frequency $f_s$ (kHz)	625	625
Feedback voltage (V)	0~5	0~5

The high-order complex  $\Sigma\Delta\text{M}$  gyroscope is a conditionally stable system as it has two control loops. Both open loop transfer function of the system can be defined by  $L=1/QNTF-1$ , determining the gyroscope stability. In fig.6(a), the amplitude bode plot illustrates this conditionally stable system as the phase lag is above 180deg for a gain above 0dB. The root locus is plotted in fig.6(b), which reveals that one pair pole moves into the unit circle with increasing quantizer gain. In order to obtain stable operation, the minimal values of the compensator coefficients of  $A$  and  $\alpha$  can be configured as 44 and 0.94, respectively.

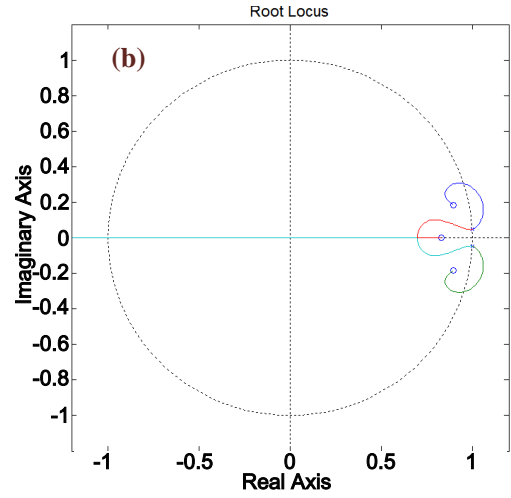
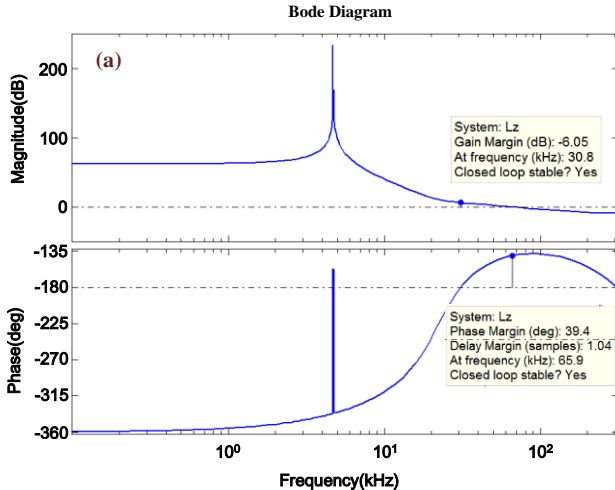


Fig. 6. Bode diagram and root locus of the single loop filter of the system.

The gyroscope sensing element studied in this work is a vibratory wheel type, that has no dedicated quadrature error electrodes and only one set of sense and feedback electrodes. Therefore, the in-phase and quadrature-phase bitstream signal must be combined and applied through only one feedback channel. A new time-division-multiplexing (TDM) mechanism which takes frames of signals and multiplexes them into a TDM frame. It requires to operating at a frequency higher than the maximum frequency used for the channels. Here, the  $Y_{Cor}(n)$  and  $Y_{Quad}(n)$  bitstreams are time-division-multiplexed (TDM), and then applied to one set feedback electrodes of gyroscope using a multiplexer, which operates at four times of the system sampling frequency ( $f_s$ ).

### III. SIMULATION ANALYSES

#### A. Noise shaping

The gyroscope overall noise performance is determined by the mechanical noise of the gyroscope sensing element, the electronic noise and the quantization noise. To calculate the dominant output noise in the modulation system, the spectral density of the noise source can be found by multiplying the noise source spectral density with the modulus of the transfer function. The expressions can be calculated as:

$$M(f) = |STF| \times M_1(f) \quad (15)$$

$$E(f) = |ENTF| \times E_1(f) \quad (16)$$

$$Q(f) = |QNTF| \times (Q_1(f) + Q_2(f)) \quad (17)$$

where  $M(f)$ ,  $E(f)$  and  $Q(f)$  is the mechanical noise, electronic noise and multi-bit quantization noise spectral density. The spectral density of the noise sources are shown in Fig.7. It can be observed that there is only one notch in the  $ENTF$  and  $QNTF$ , which is determined by the poles of the gyroscope sensing element and sigma-delta local resonator. The notch denotes the band-pass characteristics centered at 4.6kHz. The electronic noise is still the system performance limiter, and quantization noise is determined by the resolution of the multi-bit quantizer.  $1/f$  noise does not significantly contribute to the overall noise floor due to the angular rate signal being synchronously modulated by the drive signal within bandwidth; furthermore, carrier wave or chopping modulation techniques in front-end

analog circuit are effective to remove  $1/f$  noise and offset.

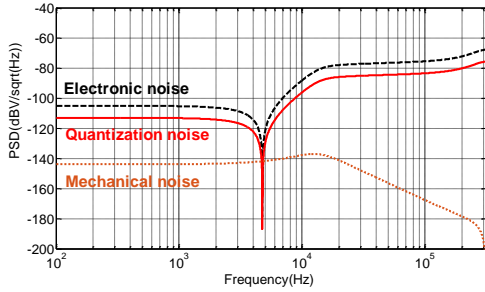


Fig. 7. Spectral density of the modulation output noise: electronic noise (black dashed line), quantization noise (red solid line) and mechanical noise (Brown dashed line).

**B. Quadrature error cancellation**

The behavioral model of the system in Fig.3 is constructed using Simulink. It is difficult to exactly pinpoint the sources for the quadrature error; the most likely reasons are any asymmetry in the mechanical vibrating mass springs, damping and electrostatic driving force. Simulated mass imbalances are changed by factors of 1/50, 1/60 and 1/100, representing the ratio of the effective sensing to driving mass. Simulated quadrature errors are lower than  $10^\circ/s$  (expressed as equivalent of angular rate). The nominal  $2\mu m$  capacitive gaps of the drive fingers are modified to  $2.2\mu m$  in the simulation, which yield a quadrature error of  $100^\circ/s$ . Any imbalance due to damping can be practically neglected since damping is strongly suppressed by vacuum packaging. The most important quadrature error source is spring imbalance, originating from a variation in the structural beam width due to micro-fabrication tolerances. The effects of spring imbalances also can be simulated each time by modifying the width by  $0.5\mu m$ , resulting in a quadrature error signal larger than  $200^\circ/s$ . Therefore, we here choose  $0.0001^\circ$  off-axis proof mass displacement as the cumulative effect of the quadrature error in simulation. The simulated output spectrum of the proposed gyroscope system including this quadrature error is shown in Fig.8. The simulated final noise shaping notch is centered at  $4700Hz$ , which is the same as the sense resonant frequency  $f_y$ . The quadrature error signal is located at the center frequency and is equivalent to an angular rate amplitude of approximately  $200^\circ/s$ . The simulation result shows an 80dB attenuation of the quadrature error in the proposed complex  $\Sigma\Delta M$  gyroscope system.

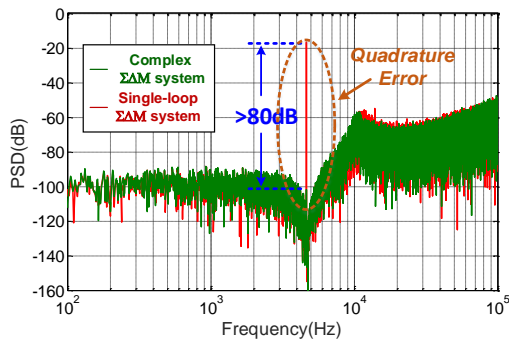


Fig. 8. Simulated output PSD of the complex EM- $\Sigma\Delta M$  system (green) and single-loop EM- $\Sigma\Delta M$  system (red). An attenuation of over 80dB of gyroscope quadrature error signal was achieved in a Simulink model.

**C. Nonlinear feedback optimization**

For an ideal electronic  $\Sigma\Delta M$ , there exists less nonlinearity due to its inherent linearity of the feedback signal. However, an electromechanical  $\Sigma\Delta M$  system includes a micromechanical sensing element with a finite resonant frequency which leads to a relatively low dc gain within the signal band. Electrostatic feedback is applied by means of a digital pulse train. The pulse train results in a periodic motion of the proof mass around the equilibrium condition, even under zero external angular rate. This movement of the proof mass cannot be separated from an external input and appears as noise or dead-zone, which can be represented as

$$\Delta y = \frac{\Omega_{max}}{(2\pi \times (f_s / 4))^2} \tag{18}$$

Notice that the nonlinearity source is inversely proportional to  $f_s^2$ , whereas the other noise sources are inversely proportional to  $f_s$ . Therefore, this error source decreases considerably for high sampling frequency  $f_s$ .

Although digital plus applies with some constant voltages, the generated electrostatic force is nonlinear as it has higher harmonic content relating to the residual motion, leading to a reduction in SNR. The spectrum in response to an input angular rate  $\Omega(t)$  with  $200^\circ/s$  amplitude and  $64Hz$  frequency is shown in Fig.9. It is obviously that there are odd (3, 5...) harmonic distortion peaks with respect to the residual motion. An effective force linearization scheme is proposed in [12], which can be used to decrease nonlinearity and thus increase SNR. The linearity of the gyroscope system was investigated by simulation over an angular rate input range of  $\pm 300^\circ/s$ . The maximum nonlinearity was found to be 0.0184%, as shown in Fig.10.

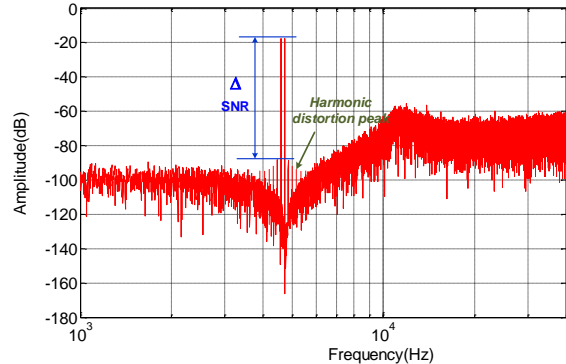


Fig. 9. Output spectrum of gyroscope with nonlinearity feedback system.

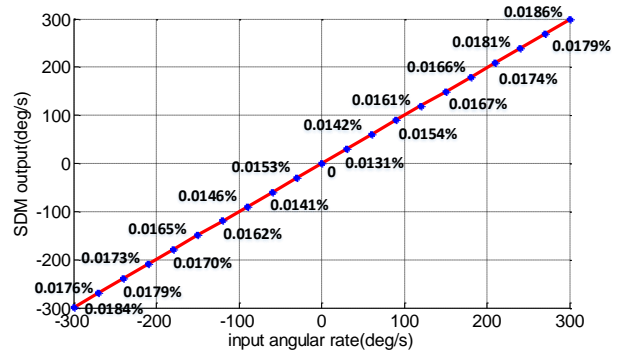


Fig. 10. Simulated linearity response of the proposed complex  $\Sigma\Delta M$  gyroscope.

#### D. Frequency-split analyses

The sensitivity of high quality factor gyroscopes is usually contradictory to frequency-split and bandwidth. Therefore, in terms of open loop control of the sense mode, usually a trade-off has to be made, and set the difference between the two resonant frequencies. Both mode-matching and electrostatic rebalancing are used together to enhance the performance. However, it is still difficult to perfectly match resonant frequencies in operation even if electrostatic tuning is used. Even small variations of the gyroscope frequency-split easily lead to a phase change of the signal. Assuming a resonant frequency mismatch of 100Hz due to microfabrication tolerances, with all other parameters as before, a simulation was carried out with the gyroscope system model. The output spectrum in Fig.11(a) shows that the input angular rate signal (200°/s, 64Hz) is no longer symmetrically mirrored at the notch center frequency ( $f_y$ ) resulting in a higher noise floor (-130dB) than if perfect mode matching is assumed (-140dB). Compared with Fig.11(b), there is nevertheless no apparent angular rate amplitude degradation even due to a 100Hz resonant frequency mismatch.

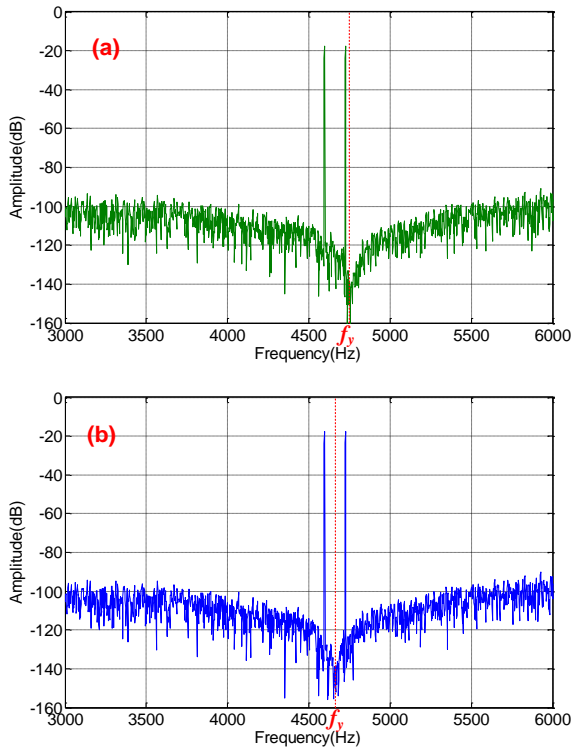


Fig. 11. Resonant frequency mismatch (a) and match (b) effect on the output spectrum of the gyroscope system with a 200°/s, 64Hz angular rate input.

### IV. IMPLEMENTATION AND TEST RESULTS

#### A. Gyroscope sensing element

As shown in Fig.12, the gyroscope used in this work is a wheel resonant structure [11]. It comprises a circular outer frame, a circular inner frame and a single central anchor. Four folded link beams are symmetrically arranged for the drive mode. The outer frame will rotate about the z-axis to achieve a large drive angle  $\theta_z$  when driven by five groups of angular

combs. If the gyroscope is subjected to an angular rate signal  $\Omega_x$  about the x-axis, the proof mass vibrates about the torsional beam and generates an angular deflection around the y-axis. The mechanical coupling between the drive and sense modes is suppressed by the high out-of-plane stiffness of the driving beam and the dual frame structure. Fig.13 shows a simplified cross section of the gyroscope. The fabrication process starts with the preparation of a SOI wafer by forming different electrodes and anchors based on a Through-Silicon-Via (TSV) technology and interconnect metallization; The 15um thick device layer is patterned on a single crystal silicon wafer using deep reactive ion etching DRIE; then, the patterned silicon wafer and SOI wafer are fusion bonded to each other. Finally, a silicon capping layer is bonded for hermetically sealed gyroscope chip at a pressure of ~0.1Pa.

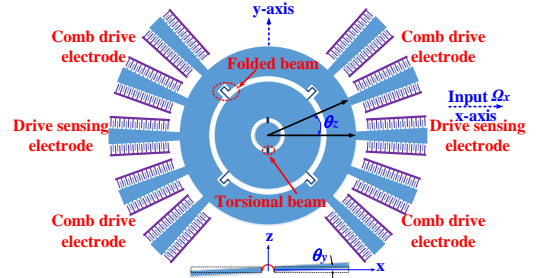


Fig. 12. Schematic view of the micromachined wheel resonant gyroscope [11] used in this work.

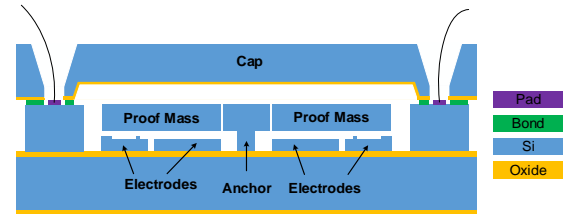


Fig. 13. Simplified cross-section of the MEMS gyroscope chip used in this work.

Ring-down tests were first carried out to accurately determine the  $Q$ -quality factor value of the packaged sensing element; test results are shown in Fig.14, indicating a resonant frequency of the gyroscope drive and sense modes of 4660Hz and 4754Hz, and corresponding quality factors of 510000 and 8000, respectively. The quality factor of the sense mode is significantly lower than of the drive mode because the dominant damping mechanism of the varying gap sensing electrodes is the squeeze film damping effect; this result in a higher damping coefficient compared to the slide film damping in the varying overlap type drive fingers. In addition, the torque created by the differential movement of the sense beam on the substrate also reduces the sense mode quality factor.

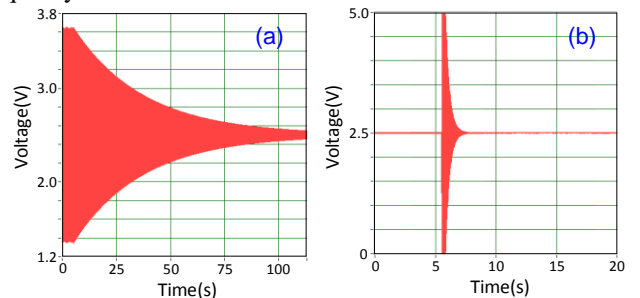


Fig. 14. Ring-down test results of the drive (a) and sense mode (b) for the MEMS gyroscope to determine the Q-quality factor.

**B. Drive oscillating system**

The drive loop needs to provide robustness to parasitic drive mechanical resonant modes of the gyroscope, and furthermore a low phase noise clock for the entire interface digital circuit system. Ideally, the drive dynamics can be represented as a single spring mass damper system in the force-to-displacement transfer function. In reality, it consists of many coupled systems with a multitude of resonant peaks as shown in Fig.15. The drive control circuit needs to lock to the correct resonant peak and reject the others even if their peak values are higher than that of the desired peak. Fig.16 shows the schematic of our designed drive control loop, which embeds a phase locked loop (PLL) inside the loop and also uses a band-pass filter to provide attenuation of gyroscope parasitic resonant modes. The PLL output clock is divided into a drive feedback force signal, self-clocking signal ( $f_{clk}$ ) and carrier wave signal ( $f_{carrier}$ ). The PLL clock operates with a DAC that produces a sinusoidal waveform to drive the gyroscope having lower harmonic content and reducing the chance of locking to parasitic modes.

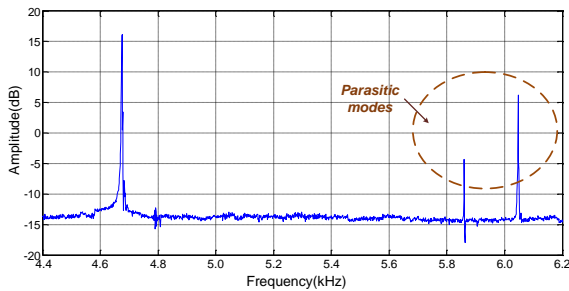


Fig. 15. Coupled spring mass damper system with multiple resonant peaks in drive mode.

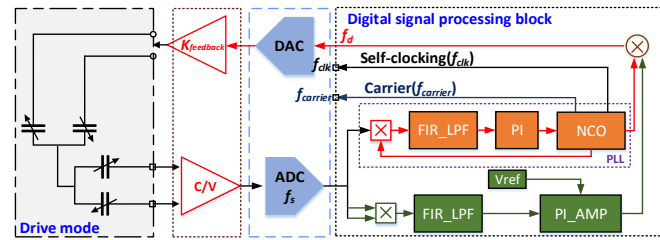


Fig. 16. Self-clocking drive loop of this work with a digital PLL embedded inside.

**C. Gyroscope prototype system**

The gyroscope chips were integrated with the proposed EM- $\Sigma\Delta$  control electronics on a printed circuit board (PCB). Fig.17 shows a photograph of the implemented gyroscope prototype system under test. The system consists of three modules: i) MEMS module comprising the sensing element, ii) analog module comprising the preamplifiers, switches and force feedback amplifiers and iii) a digital module comprising the drive mode phase locked loop and sense mode complex  $\Sigma\Delta$  force rebalancing loop. The latter includes the in-phase sigma-delta modulator, generating the electrostatic force to counter-balancing Coriolis force and the angular rate output signals as well as the quadrature-phase sigma-delta modulator for quadrature motion suppression. The whole system operates

with a single power supply of +5V and occupies an overall size of 6cm $\times$ 3cm.

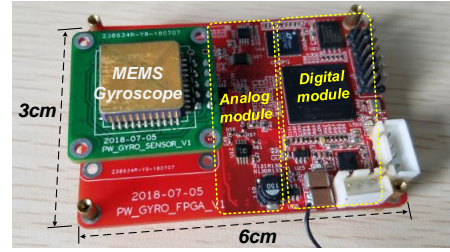


Fig. 17. Photograph of the gyroscope prototype system. The modules are hybrid integrated on a PCB with a size of 6cm $\times$ 3cm.

**D. Noise shaping with quadrature cancellation**

Before starting the measurements, the drive mode frequency tracking loop was activated to allow system to lock onto the gyroscope resonant frequency. Furthermore, the amplitude of the driving signal was set to stabilize the drive mode amplitude to a fixed value of 0.25V. We operated the gyroscopes under mode matching conditions by tuning the polarization voltage difference with a frequency-split of less than 1Hz.

The Coriolis sense loop is a discrete-time electromechanical sigma-delta modulator with all required building blocks: an analog filter in the form of a force to displacement transfer function of the MEMS sensing dynamics, sampling, integration and a quantized negative feedback. It is well known that system time delay and clock jitter will mix with the quantization noise resulting in an increased in-band noise floor [3]. The detection loop shapes this noise away from the drive frequency of 4754Hz to higher frequencies. Fig.18 shows the measured spectrum of the output bitstream, which was in good agreement with the simulation results. The higher-order parasitic notch in the measured spectrum at 5.85kHz and 6.04kHz are due to additional parasitic resonant modes. The measured noise floor was -120dB within a 64Hz bandwidth, which was 20dB higher than the simulation results. In a single-loop architecture, there is a quadrature error signal at the notch center frequency, resulting in approximately the same angular rate amplitude as a 200 $^\circ$ /s input signal. The designed complex  $\Sigma\Delta$  gyroscope system achieved an approximately 80dB cancellation of the quadrature error with feedback pulses of less than 1V, and was thus in good agreement with the simulation results.

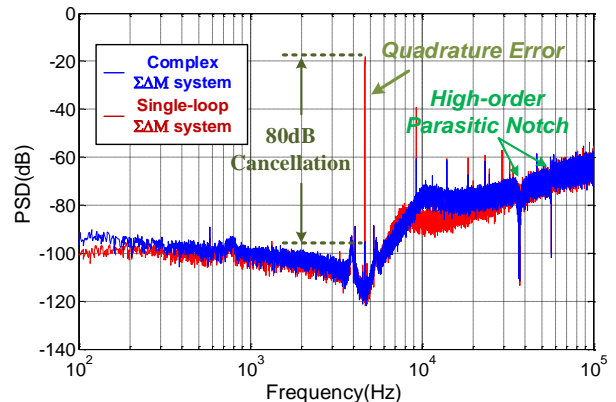


Fig. 18. Measured spectrum of the output bitstream of a single-loop (red) and the design complex EM- $\Sigma\Delta$  gyroscope (blue) achieving a quadrature error

cancellation of 80dB.

**E. Self-clocking for turn-on bias calibration**

The residual motion of the MEMS gyroscope sensing element makes the performance of the electromechanical  $\Sigma\Delta M$  easy suffer from non-ideal feedback pulse shapes. Therefore, a low-jitter clock is necessary for high-precision closed-loop control. The peripheral circuit system includes a digital PLL that generates a reference clock using the high quality factor drive resonance of the gyroscope. This result in a self-clocking scheme, thus an external crystal is not required. Moreover, a major drift source for the gyroscope is their inherent sensitivity to temperature variations. The drive resonance frequency can be regarded as an inherent thermometer, which is free from any spatial or temporal thermal lag. This self-clocking technique allows fixing the ratio between the system sampling frequency ( $f_s$ ) and the drive mode resonance frequency ( $f_x$ ); this not only enables interfacing to a wide-range of sensor modules but also self-sensing and compensating the gyroscope temperature drift.

We demonstrate that the gyroscope self-heating induced turn-on bias drift can be reduced by the proposed approach. During turn-on the electronics and mechanical resonators heat up due to a temperature gradient across the gyroscope system. Fig.19 presents the measured output bias drift of the proposed gyroscope with and without self-clocking scheme, respectively. A strong correlation can also be observed for bias as a function of the gyroscope resonance frequency. Self-clocking removed the linear trend and enabled a total bias error of 3 %h during 1800s of the temperature ramp-up since cold start, proving feasibility of the approach. The measurements are obtained for two conditions: with and without quadrature cancellation. The complex EM- $\Sigma\Delta M$  gyroscope bias error decreases by two to three orders of magnitude. This is due to the fact that the signal processing units in electronics become more accurate with the quadrature suppression.

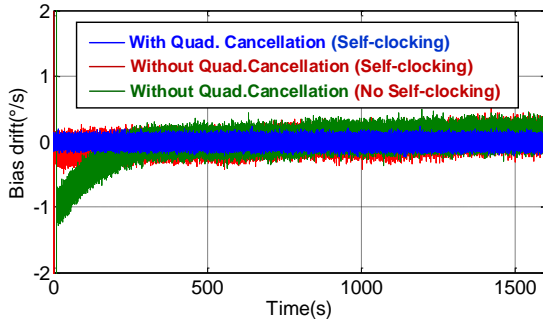


Fig. 19. Measured the bias output of self-clocking EM- $\Sigma\Delta M$  gyroscope system with and without quadrature cancellation during power-on.

**F. Gyroscope performance**

The gyroscope prototype system was tested and Fig.20 shows the measured Coriolis output signal versus applied rotation  $\Omega$  with and without quadrature error cancellation. The rotation was varied over an interval of  $\pm 300^\circ/s$ . Scale factor with quadrature error cancellation (2174LSB/ $^\circ/s$ ) is slightly higher than the system without quadrature cancellation (2073LSB/ $^\circ/s$ ). That is due to quadrature and in-phase errors leak more into the sense channel in a conventional single loop

$\Sigma\Delta M$  gyroscope. The result of a best line fit on the measurement results indicates that the full scale ( $\pm 300^\circ/s$ ) maximum nonlinearity error of the gyroscope is less than 0.021% with the  $\Sigma\Delta M$  quadrature cancellation loop.

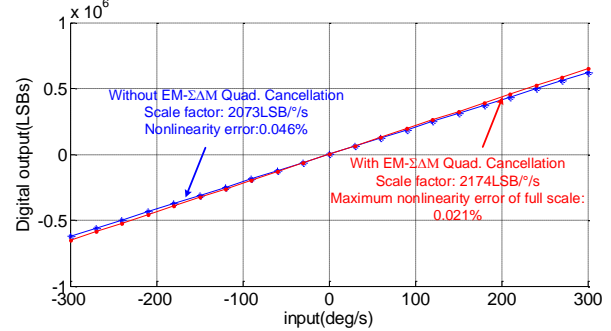


Fig. 20. Measured output digital reading versus input rotation rate with and without the quadrature error cancellation. The maximum nonlinearity errors of gyroscope full scale ( $\pm 300^\circ/s$ ) improves by a factor of 2X with the quadrature cancellation.

To perform a long term stability analysis, the gyroscope prototype static measurements (zero rate output) was recorded for a period up to 24h at room temperature. An Allan deviation analysis allows determination of random processes present in the zero-rate output signal. Fig.21 shows Allan variance graphs of the gyroscope prototype with and without quadrature cancellation. The bias instability of the zero rate output was improved from 5 %h to 0.9 %h with increasing averaging time, indicating a 5.5-fold performance improvement, and thus confirming the advantages of the propose method. The angle random walk (ARW) of the gyroscope system with sigma-delta quadrature cancellation was also measured, exhibiting a 3-fold improvement compared to the gyroscope without quadrature cancellation. Besides, it also indicates that the long-term drift is effectively reduced after self-clocking compensation. Results indicated here that a lower quadrature error, better zero rate output and ARW performance were achieved, thus resulting in significant overall gyroscope performance improvements. The gyroscope bandwidth was not affected by the quadrature cancellation loop since the prototype system bandwidth is determined by the electronic filter stage in the sense-mode electronics.

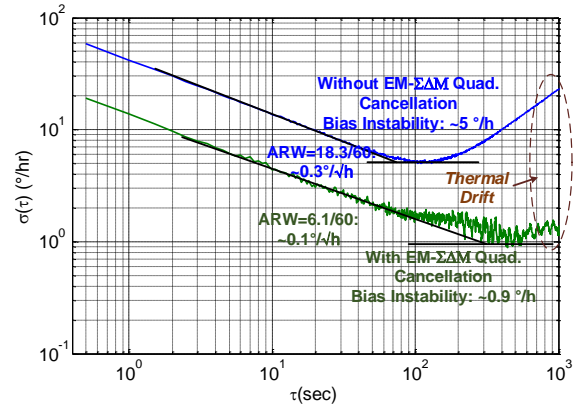


Fig. 21. Allan deviation of EM- $\Sigma\Delta M$  gyroscope prototype output with and without quadrature error cancellation.

## V. CONCLUSIONS

A complex EM- $\Sigma\Delta$  force rebalanced sensing scheme with quadrature error cancellation was described for a MEMS gyroscope. The proposed scheme allows gyroscope sensing signal in-phase and quadrature-phase decomposition to realize sigma-delta noise shaping and error cancellation. Rather than using dedicated mechanical electrodes, the Coriolis force and quadrature force signals are high-order band-pass sigma-delta modulated and counter rebalanced, respectively. Simulations showed that the anisotropic mechanical sensing element causes a higher quadrature error, and feedback nonlinear and robust optimized were used adopted to enhance the performance of the gyroscope. Consequently, in output bitstreams, the quadrature forces are cancelled to provide an inherently high-SNR signal, as compared to the conventional single-loop EM- $\Sigma\Delta$  scheme. Furthermore, the self-clocking scheme based on PLL provides a self-compensation of the gyroscope turn-on drift by utilizing its resonant frequency as a built-in thermometer.

The experimental investigations of the gyroscope showed that an approximately 80dB cancellation of the quadrature error was achieved with pulses voltage less than 1V. Tests performed with and without the sigma-delta quadrature error cancellation showed that the bias instability (BI) and ARW achieved 0.9 %h and 0.1 %  $\sqrt{h}$  with improvement factors of 5.5X and 3X compared to gyroscope system without quadrature cancellation, respectively. Out bias error improved up to three orders of magnitude with the quadrature control loop. It enabled a total bias error of 1 %h and a total nonlinearity error of 0.023%. The demonstrated  $\Sigma\Delta$  force rebalancing method provides a path for sub-degree inertial-grade silicon MEMS gyroscopes.

## REFERENCES

- [1] A. M. Shkel, "Precision navigation and timing enabled by micro technology: Are we there yet?" *Proc. SPIE*, vol. 8031, pp. 803118, May. 2011.
- [2] M. Weinberg and A. Kourepenis, "Error sources in in-plane silicon tuning-fork MEMS gyroscopes," *J. Microelectromech. Syst.*, vol. 15, no. 3, pp. 479-491, Jun. 2006.
- [3] F. Chen, X. Li, and M. Kraft, "Electromechanical sigma-delta modulators ( $\Sigma\Delta$ ) force feedback interfaces for capacitive MEMS inertial sensors: A review" *IEEE Sensors J.*, vol. 16, no. 17, pp. 6476-6495, Sep. 2016.
- [4] F. Chen, W. Zhou, H.S. Zou, M. Kraft, and X. Li, "Self-clocked dual-resonator micromachined Lorentz force magnetometer based on electromechanical sigma-delta modulation," in *Proc. 31st IEEE Int. Conf. MEMS*, Belfast, UK, Jan.2018, pp. 940-943.
- [5] F. Chen, Y. Zhao, J. Wang, H. Zou, M. Kraft, and X. Li "A single-side fabricated triaxis (111)-silicon microaccelerometer with electro mechanical sigma-delta modulation," *IEEE Sensors J.*, vo.18, no.5, pp.1859-1869, Mar.2018
- [6] V. P. Petkov and B. E. Boser, "A fourth-order SD interface for micromachined inertial sensors," *IEEE J. Solid-State Circuits*, vol. 40, no. 8, pp. 1602-1609, Aug. 2005.
- [7] M. Saukoski, L. Aaltonen, and K. A. I. Halonen, "Zero-rate output and quadrature compensation in vibratory MEMS gyroscopes," *IEEE Sens. J.*, vol. 7, no. 12, pp. 1639-1652, Dec. 2007.
- [8] J. A. Geen, S. J. Sherman, J. F. Chang, and S. R. Lewis, "Single-chip surface micromachined integrated gyroscope with 50 %h Allan deviation," *IEEE J. Solid-State Circuits*, vol. 37, no. 23, pp. 1860-1866, Dec. 2002.
- [9] E. Tatar, S. E. Alper, and T. Akin, "Quadrature error compensation and corresponding effects on the performance of fully decoupled MEMS gyroscopes," *J. Microelectromech. Syst.*, vol. 21, no. 3, pp. 656-667, Jun. 2012.
- [10] F. Chen, J. Gu, P. Salimi, M. Kraft, and X. Li, "Self-clocking electro-mechanical sigma-delta modulator quadrature error cancellation for MEMS gyroscope," in *Proc. 32nd IEEE Int. Conf. MEMS*, Seoul, Korea (South), Jan.2019, pp. 700-703.
- [11] B. Sheng, F. Chen, C. Qian, D. Xu, S. Guo, and X. Li, " Design of a dual quantization electromechanical sigma-delta modulator MEMS vibratory wheel gyroscope," *J. Microelectromech. Syst.*, vol. 27, no. 2, pp. 218-230, Apr. 2018.
- [12] F. Chen, H. Chang, W. Yuan, R. Wilcock, and M. Kraft, " Parameter optimization for a high-order band-pass continuous-time sigma-delta modulator MEMS gyroscope using a genetic algorithm approach," *J. Micromech. Microeng.*, vol. 22, no. 10, Art.no. 105006, Oct. 2012.
- [13] Y. Dong, M. Kraft, and W. Redman-White, "Force feedback linearization for higher-order electromechanical sigma-delta modulators," *J. Micromech. Microeng.*, vol. 16, no. 6, pp. S54-S60, 2006.